ACS APPLIED NANO MATERIALS

www.acsanm.org Article

Nanolaminate Plasmonic Substrates for High-Throughput Living Cell SERS Measurements and Artificial Neural Network Classification of Cellular Drug Responses

Wonil Nam, Han Chen, Xiang Ren, Masoud Agah, Inyoung Kim, and Wei Zhou*

Cite This: *ACS Appl. Nano Mater.* 2022, 5, 10358−10368 Read Online

ACCESS | Metrics & More | Article Recommendations | Supporting Information

ABSTRACT: Rapid in situ bio-analysis of cellular behaviors in response to external stimuli remains a formidable challenge but can open crucial opportunities in biology and medicine. The standard label-based end point assays suffer from invasiveness and complex sample handling. In this regard, label-free surface-enhanced Raman spectroscopy (SERS) has emerged as a promising non-invasive in situ bio-analysis technique for living cells. Nevertheless, achieving rapid in situ SERS bio-analysis still faces challenges in reliable high-throughput measurements and accurate multivariate analysis, which requires significant innovations in bio-interfaced SERS devices and machine learning (ML) methods. Here, we exploit cell-interfaced nanolaminate SERS substrates to demonstrate reliable high-throughput SERS measurements using well-studied living cancer cells with four drug dosages. Artificial neural network (ANN) for multiclass classification of cellular drug responses provides high accuracy (94%). Uniquely, nanolaminate SERS substrates with a high SERS enhancement factor (>10^7) can rapidly generate big SERS data sets with rich molecular information on living cells (10,000 spectra within 3 min) that can enable the utilization of data-hungry ML methods (e.g., ANN). By capturing additional hidden features in high-dimensional spectroscopic data, ANN is more powerful for multiclass classification than five other popular ML methods, including principal component analysis combined with linear discriminant analysis (PCA-LDA), partial least-squares discriminant analysis (PLSDA), classification tree (CT), *k*-nearest neighbor (KNN), and support vector machine (SVM). On the basis of the proof-of-concept demonstration using drugs on living cells, we anticipate that the nanolaminate SERS substrates can potentially monitor living cell responses to other external stimuli in a label-free and non-invasive manner.

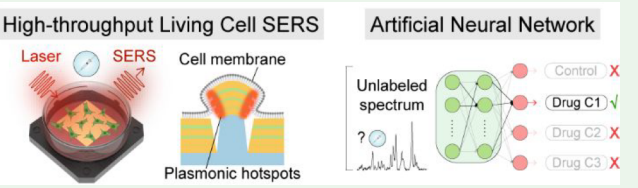

KEYWORDS: *surface-enhanced Raman spectroscopy (SERS), label-free, cancer drug response, living cell, multiclass, artificial neural network*

INTRODUCTION

Surface-enhanced Raman spectroscopy (SERS) is a technique that combines molecular fingerprint specificity of vibrational Raman spectroscopy with a high hotspot sensitivity from plasmonic metal nanostructures.[1] Given the favorable features of non-invasive measurements, minimal sample preparation, and no water background interference, SERS has become a promising biochemical analysis tool for medical diagnostics, drug testing, and environmental monitoring.[2−4] In situ label-free SERS bio-analysis of living cells has attracted increasing interest due to its potential to achieve rapid molecular profiling of cellular status without perturbing natural biological processes.[2,5] Depending on the spatial arrangement of hotspots, SERS devices can be categorized as unbound and surface-bound types.[1,6−8] Most SERS studies for living cells deploy unbound SERS devices based on discrete plasmonic nanoparticles (NP) to incorporate within cells by cellular uptake, i.e., endocytosis[9] or with specific cell membrane regions via surface functionalization.[10,11] Despite promising results, SERS measurements of living cells with unbound SERS NPs suffer from poor reliability due to challenges of (i) random NP distribution, aggregation, and diffusion, (ii) uncontrollable NP enrichment in lysosomes via the endocytic pathway,[5,9,11] and (iii) NP-related cytotoxicity.[12] On the other hand, surface-bound SERS substrates by bottom-up or top-down approaches can support dense hotspot arrays to interface with living cell cultures[13−17] but their planar surface geometries cause restrictions to achieve a tight physical coupling between hotspots and cells in SERS measurements.[18] Due to the high susceptibility of SERS enhancement factor (EF) on the relative molecule distance to hotspots,[2] uncontrollable cell adhesion with varying distances between hotspots and cell membranes on planar SERS substrates can significantly compromise the reliability to obtain a high signal-to-noise

Received: April 15, 2022
Accepted: July 19, 2022
Published: July 26, 2022

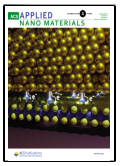

https://doi.org/10.1021/acsanm.2c01644
ACS Appl. Nano Mater. 2022, 5, 10358−10368

Scheme 1. Flow Diagram Illustration for In Situ SERS Measurements and Classification of Cellular Drug Responses: (A) Nanolaminate SERS Substrates Achievng a Tight Hotspot-Cell Coupling on 3D Protruding Nanoantennas; (B) Rapid High-Throughput 2D SERS Measurements of Living Cells Producing 10,000 Spectra within 3 min; (C) Classification of Cellular Drug Responses between Four Different Drug Dosages in a Side-by-Side Comparison between Six ML Analysis Approaches

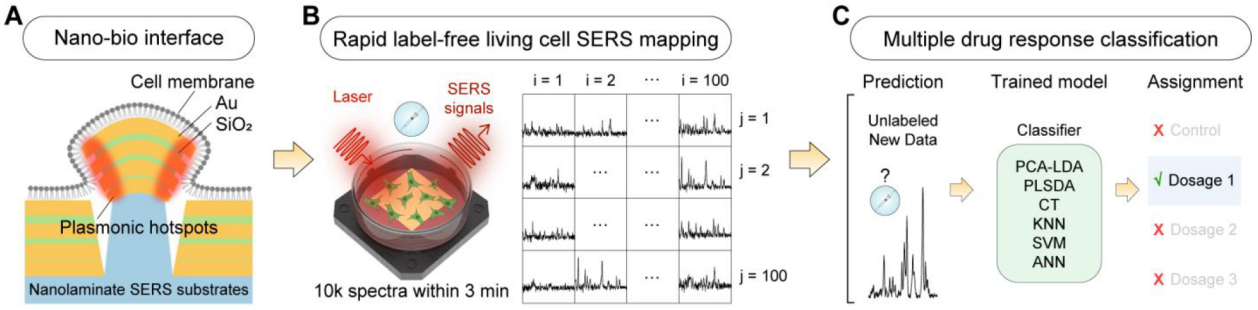

ratio (SNR) in high-throughput SERS measurements of living cells.

Recent studies have shown that 3D protruding nanotopographies can activate cellular actin reorganization to induce cell membrane engulfment behaviors.[19] The underlying mechanism is related to topography-induced membrane curvature, resulting in modulation of intracellular actin organization through curvature-sensing protein FBP17. Such nanotopography-induced cellular engulfment allowed new biomedical applications, such as in situ probing of nuclear mechanics and endocytosis processes[20,21] intracellular electrophysiology,[22,23] and optoporation-assisted intracellular delivery.[24] Despite recent efforts to create SERS substrates with 3D protruding nanotopographies to interface living cells,[18] there are no studies to achieve reliable high-throughput SERS measurements of living cells for multiclass classification of cellular responses.

Label-free SERS data sets from living cells consist of rich and complex spectroscopic features, which require machine learning (ML) analysis to extract biologically meaningful information. For example, surface proteins of living cells are heterogeneously distributed and their spatial positions and orientations change dynamically. Such variations can generate significantly varying SERS spectra profiles that are difficult to investigate by visual inspection, especially for thousands of spectra with multiple biological conditions. The majority of SERS studies have used conventional linear-based ML methods such as principal component analysis combined with linear discriminant analysis (PCA-LDA) and partial least-squares discriminant analysis (PLSDA), and high classification accuracies (>90%) have been reported for the binary classes.[25] However, no reported studies implement in situ SERS bio-analysis to classify SERS data sets among more than two cellular responses. The past decade has seen rapid development of data-hungry advanced ML methods that capture additional hidden features in big data sets for diverse applications ranging from facial/speech recognition, image analysis, analytical chemistry, and biomedicine.[26−28] Recently, artificial neural network (ANN), a branch of ML that imitates the human brain, has gained tremendous interest in SERS biochemical analysis of extracellular metabolites, bacteria lysate, and exosomes.[29−32] However, the utilization of ANN for SERS bio-analysis of living cells in multiclass classification is still rare due to the lack of sufficient training data sets that requires reliable, high-throughput in situ SERS measurements of living cells.

Assessing cellular drug responses is crucial for biomedical applications ranging from drug efficacy testing to drug resistance evolution and metabolic pathway studies. In particular, cell-culture-based tests are essential to validate the mechanism of chemotherapeutic agents before applying them to animal models or patients.[33] Conventional methods for examining cellular drug responses rely on end point biochemical assays regarding cellular apoptosis, proliferation, and cytotoxicity.[34] For example, the 3-(4,5-dimethylthiazol-2-yl)-2,5-diphenyl-2*H*-tetrazolium bromide (MTT) assay can determine cell viability and proliferation for the cell culture model.[36] Despite the strength in analytical quantification and high sensitivity, end point immunoassays have limitations of invasiveness, complex sample handling, and slow speed, restricting their capability not only in rapid bio-analysis applications but also in longitudinal studies of dynamic cellular behaviors upon drug treatment.

In this work, we exploit cell-interfaced nanolaminate SERS substrates and ANN to demonstrate reliable high-throughput SERS measurements and rapid in situ bio-analysis for multiclass classification of cellular drug responses between four dosages with high accuracy (94%, Scheme 1). A well-established breast cancer cell line, MDA-MB-231, is used to demonstrate the proof of concept. Paclitaxel (PTX), one of the most common chemotherapeutic agents for MDA-MB-231, is used with the well-known half-maximal inhibitory concentration IC_{50}. Uniquely, nanolaminate SERS substrates can support dense, uniform, intense nanogap hotspot arrays (SERS EF > 10^7) on 3D nanopillar structures to induce a tight interface between hotspots and living cells. The hotspots with combined nanoplasmonic and bio-interfaced features can enable rapid generation of big data sets with rich molecular information on living cells (10,000 SERS spectra within 3 min) from a large area (100 μm × 100 μm) that contains network-level cellular interaction activities. Such high-quality data sets allow us to leverage nonlinear-based ANN nonlinear-based to capture hidden features in complex spectral profiles beyond conventional linear-based ML methods. To our knowledge, this work is the first to perform ANN classification of label-free SERS data sets from living cells. Moreover, we compared the classification performance of ANN to five other popular ML methods, including PCA-LDA, PLSDA, *k*-nearest neighbor (KNN), classification tree (CT), and support vector machine (SVM), and ANN outperforms all others. We find that the linear-based ML methods, such as PCA-LDA and PLSDA, perform poorly with high misclassification rates, especially for drug dosages lower than IC_{50}. On the contrary, nonlinear-

https://doi.org/10.1021/acsanm.2c01644
ACS Appl. Nano Mater. 2022, 5, 10358−10368

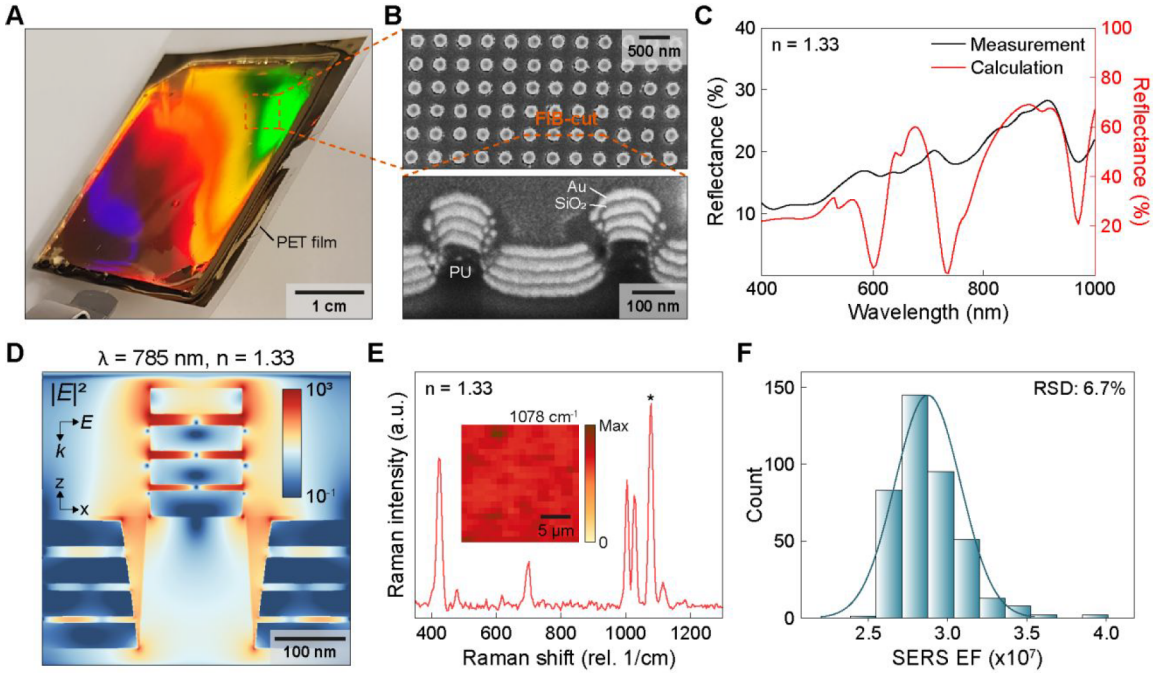

Figure 1. Optical properties and SERS performance of nanolaminate SERS substrates. (A) Photograph image. (B) Top-view (top) and cross-sectional (bottom) SEM images. (C) Measurement and FDTD-calculated reflectance spectra in the water environment. (D) FDTD-calculated distribution map of $|E|^2$ at 785 nm and n = 1.33. (E) Measured average SERS spectrum from BZT molecules functionalized nanolaminate SERS substrates. Inset: 2D Raman image using a peak 1078 cm^{-1}. (F) Histograms of SERS EFs with an RSD value of 6.7%.

based ANN exhibits much higher statistical sensitivity and specificity (90−99%) to classify the control, two sub-IC_{50}, and IC_{50} treated living cancer cells.

EXPERIMENTAL SECTION

Nanolaminate SERS Substrates Fabrication. First, we fabricated a nanowell composite polydimethylsiloxane (PDMS) stamp, a mixture of hard and soft PDMS, from a nanopillar-structured silicon wafer with a diameter of 120 nm, a height of 150 nm, and a period of 400 nm. Second, we molded the PDMS stamp with UV-curable polyurethane (PU) (NOA83H, Norland Product Inc.) to fabricate nanopillar arrays on a polyester film, which were first cured by UV for 10 min and then cured at 80 °C in a convection oven overnight. Next, we deposited alternating layers of Au and SiO_2 by electron-beam deposition (PVD250, Kurt J. Lesker Co.). The thickness of the four Au layers is 30 nm, and the thicknesses of the three SiO_2 layers are 6, 8, and 12 nm from bottom to top. Notably, we deposited 1 nm of Cr between the PU and the first layer of Au and 1 nm thick Ti between Au and SiO_2 layers as adhesion layers. Finally, we used buffered oxide etchant (BOE, 10:1) (Transene Inc.) to etch partially SiO_2 layers for 20 s.

Cell Culture and Drug Treatment. MDA-MB-231 (American Type Culture Collection, ATCC) was grown in F12:DMEM (Dulbecco's modified Eagle medium) with 4 mM glutamine, 10% fetal bovine serum (FBS), and penicillin−streptomycin (100 units per mL). Cells were grown in T-25 cm^2 culture flasks at 37 °C with 5% CO_2. Cells were detached and seeded on nanolaminate SERS substrates. The seeded cell suspension solutions were approximately 4 × 10^5 cells/mL. Paclitaxel (Sigma-Aldrich) was diluted in dimethyl sulfoxide (DMSO, ATCC) with concentrations of 1.5, 5, and 15 μM. The solutions were further diluted with 1 mL of the culture medium for the final drug concentrations of 1.5, 5, and 15 nM. For the control group, we used a culture medium that contained the same DMSO concentration as the drug treatment medium. A new medium with paclitaxel was introduced to the cells when 70% confluence was reached.

SERS Measurement. We used a confocal Raman microscope (Alpha 300 RSA+, WITec) for SERS measurements under 785 nm laser excitation (Toptica Photonics). For 2D Raman measurements of living cells, we used a 20× water immersion objective (NA = 0.5) with 10 ms integration time per pixel over a 100 μm × 100 μm area (Supporting Information Figure S1). Before the measurement, the instrumental calibration was verified by the silicon peak at 520 cm^{-1}. All measurements were conducted in the backscattering geometric configuration at room temperature. The backscatter photons were dispersed with a 300 grooves mm^{-1} (750 nm blaze grating) and detected by a CCD camera (DU-401A BR-DD-352, Andor Technology), which was thermoelectrically cooled and maintained at −60 °C.

Optical Measurement. We measured the reflectance spectrum of the nanolaminate SERS substrates in water (n, 1.33) using a UV−vis−near-IR spectrophotometer (Cary 5000, Varian).

Finite-Difference Time Domain (FDTD). We performed numerical simulations by commercial software (FDTD solution, Ansys Lumerical). A uniform mesh size of 0.5 nm (x-, y-, and z-directions) was used. The Bloch boundary condition was used in x- and y-directions with a periodicity of 400 nm, and the perfectly matched layer boundary condition was used in the z-direction. The optical constants of gold were taken from Johnson and Christy.[35]

SERS Enhancement Factor (EF). We calculated SERS EF with the equation: $EF = (I_{SERS}/I_{Raman}) \times (N_{Raman}/N_{SERS})$,[37] where I_{SERS}, I_{Raman}, N_{SERS}, and N_{Raman} are the measured SERS intensity, the neat BZT Raman intensity, and the number of BZT molecules contributing to SERS and neat Raman intensities, respectively. We used the BZT peak at 1094 cm^{-1} (in-plane C−C−C ring breathing mode with C−S stretching mode) for I_{Raman}. We used 1078 cm^{-1} for I_{SERS}, the shifted SERS peak of BZT due to the absorption onto the metallic surface. We calculated N_{SERS} using the equation $N_{SERS} = SA \times \rho_{SERS}$, where SA is the surface area of SERS substrates contributing to the enhancement of Raman signal and ρ_{SERS} is the packing density of BZT on the Au surface (6.8 × 10^{14} molecules/cm^2). We calculated N_{Raman} with the equation $N_{Raman} = Ad_{eff}\rho_{BZT}$, where A is the area of the focused illumination, d_{eff} is the effective focal depth of the beam spot, and ρ_{BZT} is the density of BZT molecules (5.9 × 10^{21} molecules/cm^3). We measured d_{eff} using a silicon wafer by changing the distance between the wafer and the objective lens.

https://doi.org/10.1021/acsanm.2c01644
ACS Appl. Nano Mater. 2022, 5, 10358−10368

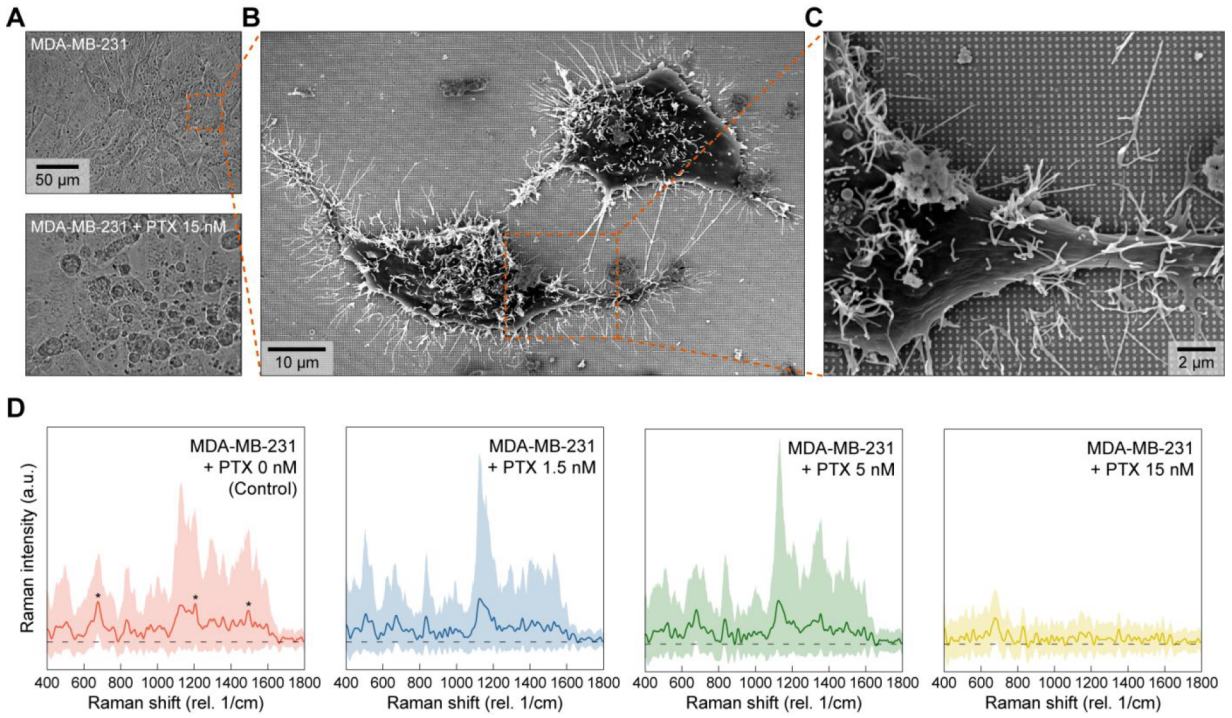

Figure 2. High-throughput in situ label-free SERS measurements of MDA-MB-231 cells cultured on nanolaminate SERS substrates. (A) Bright-field images of MDA-MB-231 control (top) and treated with PTX 15 nM (bottom). (B, C) Top-view SEM images of MDA-MB-231 on nanolaminate SERS substrates. (D) Representative average SERS spectra of cells with 5 and 95 percentiles at four different drug treatment dosages.

SERS Signal-to-Noise Ratio (SNR). We calculated SNR with the equation[38] $\mathrm{SNR} = (I_{\mathrm{SERS}} - I_{\mathrm{BG}})/\sqrt{I_{\mathrm{BG}}}$, where ISERS is the SERS intensity and I_{BG} is the background noise intensity. We identified I_{BG} in the spectral region at 2000 cm^{-1} without molecular Raman peaks. For calculating SNR values, negative I_{SERS} values were discarded.

Multivariate Machine Learning (ML) Analysis. We used the open-source R statistical software for data preprocessing and multivariate analyses. For preprocessing of SERS data sets, we first removed cosmic rays and truncated spectra from 400 to 2000 cm^{-1} within the biologically relevant region. Then, we performed baseline correction and discarded the flat spectra with no/weak Raman peaks. Specifically, spectra whose maximum peak values were smaller than three times the noise level (Figure S5) were discarded. We randomly extracted 1322 spectra from each class on the basis of the minimum number of spectra for four classes to have an equal number of spectra among different classes. To implement multivariate analyses, we used 10-fold cross-validation for all classifiers, including PCA-LDA, PLSDA, CT, KNN, SVM, and ANN. For PCA-LDA, we first generated principal components with a 95% cumulative score with the ChemoSpec package and then performed LDA with the MASS package. For PLSDA, we used the mixOmics package and conducted classification with the Mahalanobis distance. Notably, we selected Mahalanobis because it provides a higher classification accuracy than other methods using maximum and centroids distances. For CT, we used the caret and rpart packages, set the splitting as the default gini, and tuned the complexity parameter to prune trees. For KNN, we used caret and class packages, and we tuned the number of neighbors for classification in the range from 1 to 10 and selected 3 due to its minimum root-mean-square deviation value (Figure S7). For SVM, we exploited the e1071 package with the radial basis function (RBF) kernel model. Two tuning parameters, a general penalizing parameter "cost" and the RBF kernel parameter "gamma", were tuned with grid search (Figure S8), and we employed a γ value of 0.001 and a cost value of 10 that can minimize the classification accuracy error. For ANN, we used the keras package to build a neural network with two hidden layers with a widely varying number of neurons in the second layer from 4 to 150. For the activation function, we used the "sigmoid" function in the hidden layers and the "softmax" function for the output layer. An optimizer determines hyperparameter tuning in a network based on the changes from a loss function. The loss function maps the output and the true labels of the neural network onto a real number for an intuitive representation of how well the model fits the data sets. We used the "adam" optimizer, considered the best for spectral analysis,[39] with a "sparse categorical cross-entropy" loss function for the multiclass classification learning task with 128 batch size and 0.001 learning rate. Further hyperparameter tuning, such as regularization, was not needed to achieve the optimized training model.

Scanning Electron Microscope (SEM). We used FEI Helios 600 Nanolab dual-beam for focused ion beam (FIB) milling SEM imaging. For SEM of cells, cultured cells were rinsed with PBS solution twice, followed by fixation with 2.5% glutaraldehyde at room temperature for 1 h. Cells were rinsed again by PBS solution twice, followed by postfixation with 1% osmium tetroxide and dehydration in graded ethanol series from 15 to 100% (each 15 min). We used a critical point dryer for drying cells in liquid CO_2. We deposited a 5 nm PtPd layer before SEM imaging.

RESULTS AND DISCUSSION

In Situ SERS Measurements and Classification of Cellular Drug Responses. Figure 1 shows the three major steps to achieve in situ label-free SERS analysis of living cancer cells in response to different drug dosages, and we compare the performance among six different ML methods for multiclass classification of measured SERS data sets from living cells. First, to induce a tight physical coupling between hotspots and cells, we employed top-down fabricated scalable nanolaminate SERS substrates consisting of dense, uniform, and intense hotspot arrays on polymer nanopillar arrays (Figure 1A).[6,40] Nanolaminate metal−insulator−metal (MIM) nanostructures can support multiple plasmonic modes to produce dense nanoplasmonic hotspot arrays with high SERS EF (>10^7).[6,7,41] 3D protruding nanopillar structures can induce cell engulfment

https://doi.org/10.1021/acsanm.2c01644
ACS Appl. Nano Mater. 2022, 5, 10358−10368

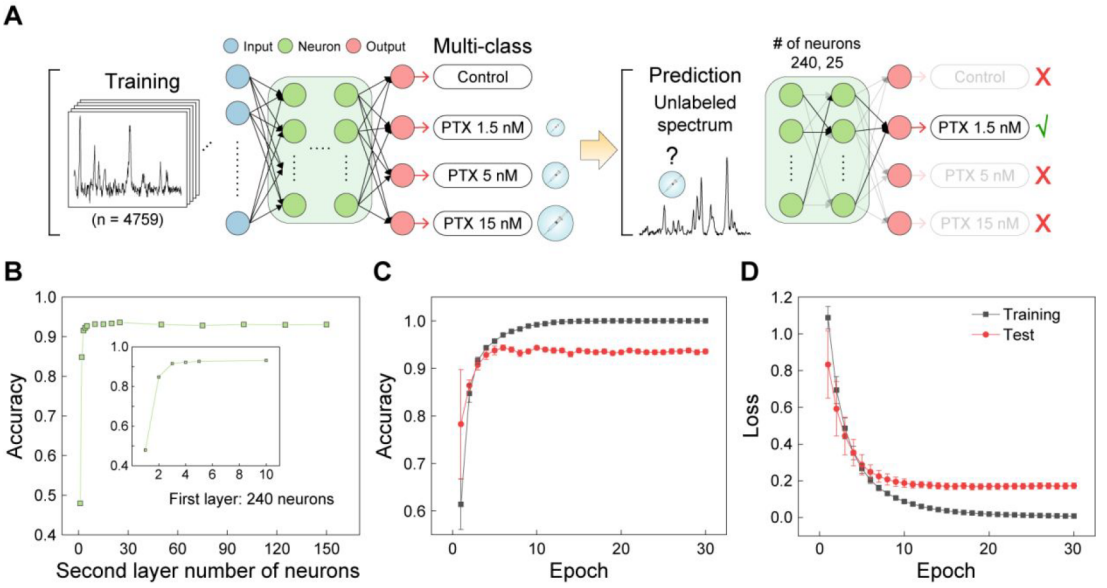

Figure 3. ANN classification with hyperparameter optimization. (A) Schematic illustration of ANN classification methods. (B) Classification accuracy as a function of the number of neurons in the second layer. (C) Accuracy and (D) loss of training and test data sets as a function of Epoch, i.e., learning iteration.

behaviors,[19] resulting in tight hotspot−cell coupling. Second, we performed in situ 2D SERS measurements of living cancer cells directly cultured on nanolaminate SERS substrates with different drug dosages, providing 10,000 spectra (10 ms per spectrum) in less than 3 min (Figure 1B). Last, we compared classification performances of six different multivariate analysis approaches using unlabeled data and found that ANN outperformed other methods with the highest classification accuracy for multiclass label-free SERS data sets from living cells (Figure 1C).

Optical Property and SERS Performance Characterization of Nanolaminate SERS Substrates. We first investigated the optical properties and SERS performance of nanolaminate SERS substrates in water to mimic the reflective index background of plasmonic nanostructures in the physiological cell culture environment. Figure 2A shows a bright-field image of a large area (~16 cm^2) of nanolaminate SERS substrate. The soft-nanolithography fabrication provides cost-effective mass production of substrates, desirable for biomedical applications (see fabrication details in Experimental Section). The vivid diffraction pattern manifests uniform periodic arrays of 3D nanoantennas in nanolaminate SERS substrates verified by a top-view SEM image in Figure 2B, top. Figure 2B, bottom is a cross-sectional SEM image obtained by FIB milling showing the nanolaminate feature with multiple Au−SiO_2 interfaces. The thicknesses of Au (30 nm) and SiO_2 (6, 8, and 12 nm from the bottom) layers were tuned to have optimal SERS performance under 785 nm excitation.[42,43] Figure 2C shows the far-field optical property of the nanolaminate SERS substrates with measured and FDTD calculated reflectances. We set a refractive index background to 1.33 to mimic the physiological environment. We observed several plasmon resonant features in reflectance spectra, and such multiresonant plasmonic property originates from the hybridization of elementary plasmonic modes in multiple vertically stacked MIM building blocks.[6] Both measurements and calculations reveal resonant dips near 785 nm in reflectance spectra to match the near-infrared 785 nm excitation laser wavelength, which is beneficial to SERS bioanalysis applications due to the reduced photodamage and low autofluorescence. As expected, the resonant spectral features in measurements show broader line width and shallower amplitude than simulations because of inhomogeneous broadening from geometric variations and homogeneous broadening from interfacial roughnesses.[44]

To investigate the near-field optical property of nanolaminate SERS substrates, we calculated an electric field distribution map of the single 3D nanoantenna unit by FDTD (Figure 2D). Under 785 nm excitation with a background refractive index of 1.33, nanolocalized optical fields concentrate in the dielectric nanogap regions and sidewalls. Cell membranes cover these regions after cellular engulfment; therefore, tight hotspot−cell coupling can improve SERS signals of extracellular molecules from living cells. We then characterized the SERS performance of nanolaminate SERS substrates using a self-assembled monolayer of benzenethiol (BZT), a nonresonant molecule under 785 nm excitation. The BZT-coated sample was immersed in water during the measurement, and 2D SERS measurements were conducted over a 20 μm × 20 μm area with 400 pixels. The average spectrum reveals the BZT-specific features, and the inset 2D Raman image shows good uniformity of the nanolaminate SERS substrates. We further calculated the SERS EF based on the equation, EF = $(I_{SERS}/I_{Raman}) \times (N_{Raman}/N_{SERS})$ (details in Experimental Section). The average SERS EF is 2.9 × 10^7, which can provide sufficient sensitivity for single-molecule detection.[37] The histogram plot shows an excellent fitting to a normal distribution curve, in good agreement with the 2D Raman mapping result in Figure 2E, and the calculated relative standard deviation of 6.7% is much lower than the typical commercially available SERS devices.[45]

High-Throughput Label-Free SERS Measurements of MDA-MB-231 Cells. We cultured a triple-negative, highly malignant breast cancer cell line, MDA-MB-231, on the nanolaminate SERS substrates. The cultured MDA-MB-231 cells on nanolaminate SERS substrates made of Au and SiO_2

https://doi.org/10.1021/acsanm.2c01644
ACS Appl. Nano Mater. 2022, 5, 10358−10368

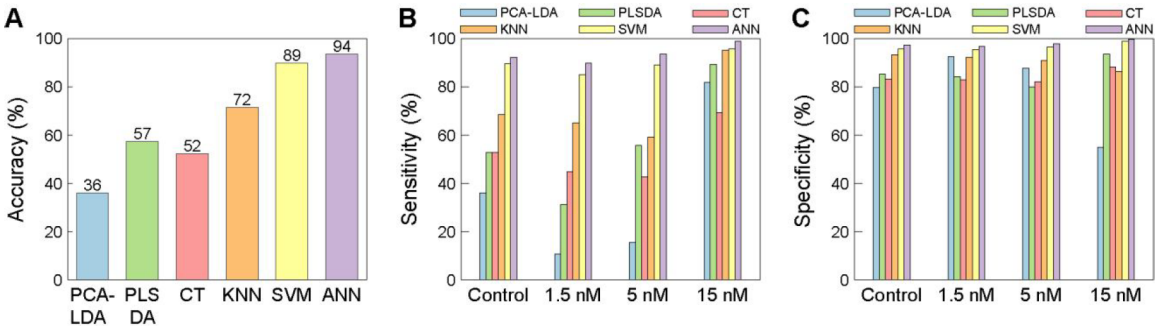

Figure 4. ANN exhibiting the best performance among six ML approaches for multiclass classification of label-free SERS data sets between cellular drug responses. (A) Classification accuracy plot for different ML classifiers. (B) Sensitivity and (C) specificity of six ML methods to classify cellular drug responses. Sensitivity and specificity represent true positive and true negative rates, respectively.

did not exhibit morphological signs of apoptosis (e.g., cell blebbing and detachment), which manifests good biocompatibility of our nanolaminate SERS substrates (Figure S2). MDA-MB-231 is a well-studied cell line to investigate breast cancer treatment.[46] The anticancer drug PTX is used in the studies, which can cause cell death by interfering with microtubules-related cell division processes.[47] Previous studies report that the IC_{50} of PTX for MDA-MB-231 is ∼15 nM.[46] Figure 3A shows bright-field images of control cells and cells treated by 15 nM PTX. The control cells exhibit a healthy spindle shape, whereas the drug-treated cells show morphologic deformities due to the mitotic arrest. Images of two other sub-IC_{50} dosages (1.5 and 5 nM) are shown in Figure S3. From SEM images of MDA-MB-231 cells in Figure 3B,C, we can observe cells sitting and covering the square pattern of nanolaminate nanoantennas with lamellipodia and filopodia at the edge of cells. Cross-sectional SEM images show cellular engulfment over nanolaminate structures, revealing that measured SERS signals mainly originate from cell membrane components (Figure S4). We performed high-throughput in situ SERS measurements for living MDA-MB-231 cells. When the cells reached ∼70% confluency, four different drug conditions, including control, 1.5, 5, and 15 nM PTX with the fresh medium, were introduced to treat the cells for 24 h. As the control, we used a culture medium containing the same DMSO concentration to dissolve PTX. The measurement data were acquired right after the sample was taken out of the incubator to minimize any side effects from the nonphysiological condition. Since nanolaminate SERS substrates allow tight physical coupling between living cells and uniform arrays of highly sensitive hotspots, we can use 10 ms integration time for each pixel to achieve rapid in situ 2D SERS measurements of living MDA-MB-231 cells with 10,000 pixels in less than 3 min over a 100 μm × 100 μm area. Based on the bright-field images, the area contains approximately 5−10 cells with varying empty areas (e.g., without cells) where secreted molecules can diffuse away from cells. Such plasmon-enhanced high-throughput reliable SERS molecular profiling of living cells can significantly increase data quality and volume. In contrast, conventional Raman measurements require high laser power and long exposure time from tens of minutes to hours to compensate for intrinsically low Raman intensity, inducing cellular photodamage to prevent in situ bio-analyses of living cells.

Figure 3D shows representative SERS spectra of MDA-MB-231 cells under four different drug dosage conditions, including control (0 nM), two sub-IC_{50} (1.5 and 5 nM), and IC_{50} (15 nM). As control experiments, we conducted SERS measurements of culture medium with and without 15 nM PTX (not including cells) with the nanolaminate SERS substrates. The measured SERS spectra did not reveal any distinct peaks in both cases due to the low PTX concentration, and the solution-based samples where medium components are unlikely to be deposited nearby SERS hotspots (Figure S5). Unlike analyte molecules such as BZT, label-free SERS spectra of living cells reveal significantly varying spectra profiles due to the dynamic biological processes and region-to-region variations. Proteins and lipids on living cell membranes are spatially heterogeneous on the nanoscale with different configurations and orientations, causing heterogeneous molecular profiles in SERS measurements over the cellular network.[2] In agreement with previous studies,[6,15,17,48] the average SERS spectra of living cells in our measurements have several common spectral features as indications of healthy cellular states, including the absence of carbon-related bands at ∼1350 and ∼1580 cm^{-1}.[49] Additionally, the three cases, including control (0 nM) and two sub-IC_{50} (1.5 and 5 nM), show similar spectral patterns in the lipid regions (∼780 to ∼890 cm^{-1} and ∼1400 to ∼1550 cm^{-1}), indicating the cancer cell property of enhanced lipid activity originated from increased fatty acid synthesis.[50] Finally, we can observe the potential presence of extracellular aromatic amino acids for cancer cells, including tyrosine (∼825, ∼1164, and ∼1178 cm^{-1}), phenylalanine (∼645 and ∼1170 cm^{-1}), and tryptophan (∼1208 and ∼1348 cm^{-1}).[51] The potential origin of SERS signals includes cell membrane components and cell-signaling molecules such as cytokines, and extracellular vesicles, including exosomes, apoptotic bodies, and microvesicles. Drug treatment can affect signaling molecule regulations and generate cell lysate components in the extracellular environment. For the regions without cells in 2D SERS measurements, molecules secreted from living cells may contribute to the acquired SERS spectra. Further in-depth spectral analysis for the IC_{50} case (15 nM) may provide molecular-level information along with cancer drug resistance evolution, which is beyond the scope of this study but deserves future investigations. Despite providing a molecular picture, direct inspection of SERS spectral features is inefficient and error-prone. Moreover, the dependence of spectral interpretation on user background knowledge can cause inevitable human bias with lab-to-lab variations. Last, the interpretation by manual spectral inspection is not feasible for multiclass classification of large-volume SERS data sets (e.g., >1000 spectra) between multiple cellular drug responses.

To evaluate the reliability of high-throughput SERS measurements for living cells, we examined the experimental

https://doi.org/10.1021/acsanm.2c01644
ACS Appl. Nano Mater. 2022, 5, 10358−10368

SNR values (details in Experimental Section). For the control cells without drug treatment, as shown in Figure S6A, three highly varying peaks (675, 1210, and 1497 cm^{-1}) revealed similar box quartile ranges with similar average SNR values of 4.35, 5.50, and 5.02. We then calculated the SNR of four different drug conditions using the 674 cm^{-1} peak, in Figure S6B. Interestingly, while 1.5 and 5 nM data sets show similar and weaker SNR values than the control data set, the 15 nM data set exhibits the lowest average SNR value of 1.79 with a shorter box quartile range. We observed a similar trend for the 1210 cm^{-1} peak (Figure S6C). The gradual decrease of SNR values with increased drug dosage is likely due to the weaker cell−hotspot coupling and increased cell death at higher drug dosage. Our observations demonstrate the feasibility of conducting rapid high-throughput SERS measurements of living cells with sufficient SNR to capture their molecular profiles.

Multiclass Classification of Cellular Drug Responses by ANN. Multiclass classification of complicated spectroscopic data sets requires multivariate ML methods.[2] We conducted a side-by-side comparison study using ANN and five other popular ML methods to classify SERS data sets from living cells under multiple drug treatment conditions. Figure 4A shows a scheme for the general mechanism of ANN. ANN consists of artificial neurons (green circles) that are the fundamental processing unit mimicking the function of biological neurons and are layered to learn information from the input. Each neuron in a layer is linked to all neurons in the next layer with weighted connections (black arrows). The artificial neurons calculate the sum of the weighted inputs and bias, subsequently providing outputs by a nonlinear activation function. A normalized exponential (softmax) function was used for the output classification tasks with non-negative probabilistic values over classes. The initial weights are randomly generated. The training model then keeps adjusting the weights in a supervised manner until the error between the true labels and predicted results is minimized. By connecting the neurons, we build a feed-forward network with hidden layers (black box) and use the final output layer to provide prediction results. Such advanced multilevel feature extraction based on the complex layer architecture allows ANN to learn the underlying critical information and nonlinear behaviors hidden in the patterns and transform the raw data feature into a high-level representation to identify class differences.[52] We trained the ANN model using four classes with different drug treatment conditions. After discarding blank or invalid spectra with no or weak Raman peaks, a total of 5288 spectra were used with balanced data distribution (1322 for each) and randomly divided into train and test sets with a 9:1 ratio. Then, we fed the unlabeled new spectrum into the trained model with the optimized hyperparameters (Figure 4A, right), including the optimum weight values depicted as black arrows. Finally, the output layer provides class assignments for the input test data sets.

Fine-tuning hyperparameters is critical to avoid overfitting or underfitting in the training model, which can misinterpret results and mislead biological decisions. For ANN, the fully connected layers require many trained weights that rely on the number of neurons in layers, and an inappropriate number of neurons can negatively affect the training model performance. For data sets with more variables than the number of input spectra, the hidden layers in a black box can easily overfit to cause high training-to-training variations.[53] Typical label-free SERS data sets from living systems can be easily overfitted using ANN approaches due to the lack of reliable high-throughput SERS measurements of living cells with sufficient SNR. Thus, previous works preferred conventional linear-based ML methods for binary cases or required additional statistical methods such as data reduction by PCA and variational autoencoder to enable multiclass classification.[30,31,54] As a validation step, we tuned the number of neurons to optimize the performance of ANN. If a single layer is used only, the number of neurons should be as high as the number of training samples to learn inputs sufficiently.[55] In this work, we used two hidden layers to significantly reduce the required number of neurons and improve computational efficiency. It has been reported that the level of abstractive representation for outputs improves as the number of layers in the black box increases.[32] For the optimum two-layer-based ANN, the number of neurons for the first layer was set to 240 on the basis of the equation[55] $2\sqrt{(m+2)N} + 2\sqrt{N/(m+2)}$, where m is the number of output neurons (i.e., the number of classes) and N is the number of spectra. Figure 4B shows the classification accuracy for four classes as a function of the number of neurons in the second layer. The classification accuracy rapidly increases to 4 neurons with 92.25% and then reveals a saturation trend with a subtle, gradual increase to 25 neurons with 93.59%. From 25 to 150 neurons, the accuracy does not change significantly with less than 0.05% differences. We finalized the number of neurons in the second layer to 25 to balance the performance with the computation efficiency. Therefore, given large SERS training data sets (>∼1000 spectra) with sufficient data quality (SNR > ∼4), we do not need a deep learning architecture consisting of more than three hidden layers to achieve successful classification of SERS data sets between four cellular drug responses, helping to reduce the computational load in ML. However, a deep neural network may be essential for in situ SERS bio-analysis to handle more complicated cellular drug testing tasks with many drug treatment conditions in drug dosages and multidrug combinations.

To assess whether the trained ANN model is over-/underfitted, we further calculated accuracy (Figure 4C) and loss (Figure 4D) as a function of Epoch number (i.e., learning iteration). The fitting status of the model can be monitored and evaluated by comparing performance curves between training and test data sets.[32,39] Regarding the accuracy curve, overfitting can occur if the training accuracy is significantly higher than the test. Also, underfitting can happen if the accuracy of the training is too low or the accuracy difference between training and test is negligibly slight. As shown in Figure 4C, the accuracy difference is saturated and stabilized from 10 learning iterations, indicating a well-fitted model. As for the loss curve, we aim to optimize the neural network learning process by minimizing the loss of the test and the distance between the training and test data sets. In Figure 4D, we calculated the sparse categorical cross-entropy loss between true labels and predicted labels as a function of the Epoch number. To achieve multiclass classification (>two classes), we employed categorical cross-entropy and the sparse model to label classes as integers. Loss of test rapidly drops to Epoch of 10 and then stabilizes, and the distance between training and test gradually increases from 10 to 30 Epoch. Evaluation of the loss curve is one of the most straightforward steps to monitoring the learning process, providing a guide for further

https://doi.org/10.1021/acsanm.2c01644
ACS Appl. Nano Mater. 2022, 5, 10358−10368

hyperparameter tuning to avoid over-/underfitting. To learn more details on neural network optimization processes to handle spectroscopic data sets, we refer readers to recent reviews.[32,39] Considering accuracy and loss curves, we used Epoch of 10 in the finalized ANN model. We find that the trained model is well-fitted with stable convergence and does not reveal significant over-/underfitting issues. Furthermore, the absence of loss fluctuations implies that the model can successfully learn the complex features from SERS spectroscopic data sets of living cells; otherwise, random features would result in a noise-like loss curve with significant fluctuations.

Comparison of Statistical Performance for Multiclass Classification. To evaluate the relative advantage of using ANN for in situ SERS bio-analysis of living cells, we compared its multiclass classification performance with several other popular ML approaches, including PCA-LDA, PLSDA, CT, KNN, and SVM. Standard deviations values of 10-fold cross-validation are shown in Table S1. PCA-LDA and PLSDA are the conventional chemometrics ML classification methods for spectroscopic data sets and are suitable for capturing linear correlations and patterns in data sets.[25,32] In Figure 5A, PCA-LDA and PLSDA show 36% and 57% classification accuracies, respectively, for the four classes of living cancer cells with different drug dosages. Compared to ANN, the significantly lower accuracies of PCA-LDA and PLSDA are likely associated with their intrinsic limitations due to the incapability to capture nonlinear hidden features in SERS data sets. On the other hand, CT, KNN, and SVM show different classification accuracies of 52, 72, and 89%, respectively, associated with the performance of their different base functions. Specifically, CT is a tree-based classification method.[56] KNN is a distance-based method with k nearest neighbors, where k is the number of neighbors.[56] SVM is an optimization-based discrimination model to generate optimal hyperplanes to separate different classes.[57] To prevent overfitting and fairly compare different methods, we performed hyperparameter optimization for KNN and SVM (Figures S7 and S8). The confusion matrix for each classifier with the raw number of spectra is shown in Figure S9.

As shown in Figure 4A, CT exhibits a low classification accuracy of 52%, reflecting that the decision mechanism based on the splitting rule can suffer from the statistical susceptibility bias for SERS data sets featured with significant internal spectrum-to-spectrum variations. Indeed, the subtle changes in data sets can evolve into a significantly different tree structure, and such statistical instability susceptible to data input variations is one of the critical limitations of tree-based classifiers. KNN reveals a classification accuracy of 72%, higher than linear-based PCA-LDA and PLS-DA methods and the tree-based CT approach. KNN employs a distance metric (e.g., Euclidean distance) to search its neighbors and can perform well when using a small number of features in determining the distance. However, the performance of KNN becomes worse if the model involves too many variables to handle high-dimensional data structures, such as the multiclass label-free SERS data sets from living cells with many Raman peaks of varying shapes and amplitudes. SVM provides 89% classification accuracy, higher than all other methods except ANN. SVM produces nonlinear boundaries by constructing linear boundaries in ample transformed feature space with kernel tricks to distinguish partly overlapped classes with slack variables.[57] The performance of SVM depends on kernel functions and tuning parameters, and we used "cost", the general penalizing parameter, and "gamma", the radial basis function (RBF) kernel parameter. To achieve the maximum classification accuracy, we tuned two tuning parameters with a grid search (Figure S8). The potential reason for high SVM classification accuracy is attributed to its utilization of hinge loss, where assignments inside each class do not play a significant role in creating boundaries, and critical differences among classes are highlighted.[57] The optimized ANN shows a higher classification accuracy of 94% than all other methods. We calculated the F1 score and acquired 0.94 for the ANN model to measure how successful a classifier is for multiclass classification. Although SVM also has a good classification accuracy of 89%, we anticipate that ANN will outperform SVM to handle more classes of SERS data sets because SVM faces intrinsic challenges in determining boundaries between high-dimensional spectral data sets, also known as the curse of dimensionality.[25]

To further evaluate the classification performance, we determined "sensitivity" by TP/(TP + FN) (e.g., the true positive rate) and "specificity" by TN/(TN + FP) (e.g., the true negative rate), respectively (Figures 4B,C), where TP is the true positive, FN is the false negative, TN is the true negative, and FP is the false positive. Overall, the sensitivity and specificity values show similar trends among different classification methods compared to the accuracy. Interestingly, PCA-LDA shows very low sensitivities of 10.6 and 15.6% for 1.5 and 5 nM, respectively. On the other hand, the PCA-LDA classifier has a sensitivity of 36% for control, similar to its classification accuracy value of 36%, but with a significantly higher sensitivity of 81.9% for 15 nM. These results indicate that the PCA-LDA classifier cannot distinguish two drug dosages lower than IC_{50} due to its limitation in capturing hidden nonlinear patterns in high-dimensional data sets. PLSDA also shows a low sensitivity of 31.1% for 1.5 nM compared to its classification accuracy of 57%. Among different drug dosage classes, all six ML methods show the highest sensitivity values for 15 nM, reflecting more distinct changes in molecular features of living cancer cells in response to a high drug concentration of the anticancer drug. Due to its powerful feature extraction capability, ANN shows the highest values for all four classes.

Regarding specificity, ANN provides an average of 98% that can effectively identify the true negative cases with minimized false-positive cases. Other methods show less reliable results than ANN. PCA-LDA exhibits the lowest specificity of 54.8% for 15 nM. Using a classifier with a low specificity would be very risky to classify cancer drug response, which will designate patients to the wrong treatment decision. The incorrect assessment of cancer drug response can cause unwanted drug resistance evolution and complicate patient body reaction during the treatment.[58] Given the sensitivity and specificity results, we believe that the linear-based methods (PCA-LDA and PLSDA) and two nonlinear-based methods (CT and KNN) are unsuitable for classifying drug responses of living cancer cells. SVM reveals a comparable but slightly poorer classification performance than ANN. Our study suggests that ANN is suitable and robust for handling complex label-free spectral data sets by capturing additional hidden nonlinear patterns in high-dimensional SERS data sets, showing promising potential in drug efficacy studies with living cancer cells.

https://doi.org/10.1021/acsanm.2c01644
ACS Appl. Nano Mater. 2022, 5, 10358−10368

CONCLUSIONS

We exploit cell-interfaced nanolaminate SERS substrates to demonstrate reliable high-throughput SERS measurements. The nanolaminate SERS substrates with a high SERS EF ($>10^7$) with excellent uniformity generated rich molecular information from living cells (10,000 spectra within 3 min). We demonstrate that ANN-based ML can empower in situ SERS profiling of living cancer cells to classify cellular drug responses between four dosage conditions with excellent multiclass classification performance in accuracy, sensitivity, and specificity. A side-by-side comparative study reveals that ANN performs better in the multiclass classification of SERS data sets than five other popular ML approaches, including PCA-LDA, PLSDA, CT, KNN, and SVM. Our results suggest that, given sufficient training data, ANN can enjoy the benefits of capturing rich hidden features in complex high-dimensional spectroscopic profiles to achieve high-accuracy multiclass classification and prediction of cellular drug responses. Without the requirement of preknowledge, additional statistical processing, and complex deep learning architecture, ANN can serve as a desirable ML method to empower rapid in situ SERS bio-analysis of cells and other biological samples. Notably, this study demonstrates the feasibility of implementing ANN-empowered in situ SERS bio-analysis to classify cellular responses under different drug treatment conditions, including drug dosages, drug exposure times, and multidrug combinations. In addition, user-friendly ANN open-source libraries are increasingly available to reduce unwanted operational variations in the ML modeling and parameter tuning process. Therefore, we anticipate that data-hungry but more powerful ML methods, such as ANN, will play an increasingly important role in supporting high-throughput SERS measurements to handle large SERS data sets for multiclass bio-analysis of living systems. Furthermore, the nanolaminate SERS substrates can potentially monitor living cell responses to other external stimuli in a label-free and noninvasive manner.

ASSOCIATED CONTENT

Supporting Information

The Supporting Information is available free of charge at https://pubs.acs.org/doi/10.1021/acsanm.2c01644.

Bright-field images of MDA-MB-231 treated by PTX 1.5 nM and 5 nM; SNR values; hyperparameter optimization for KNN and SVM; confusion matrices of six different classifiers (PDF)

AUTHOR INFORMATION

Corresponding Author

Wei Zhou − *Department of Electrical and Computer Engineering, Virginia Tech, Blacksburg, Virginia 24061, United States;* orcid.org/0000-0002-5257-3885; Email: wzh@vt.edu

Authors

Wonil Nam − *Department of Electrical and Computer Engineering, Virginia Tech, Blacksburg, Virginia 24061, United States;* orcid.org/0000-0002-7804-3049

Han Chen − *Department of Statistics, Virginia Tech, Blacksburg, Virginia 24061, United States*

Xiang Ren − *Department of Electrical and Computer Engineering, Virginia Tech, Blacksburg, Virginia 24061, United States;* orcid.org/0000-0002-8882-6362

Masoud Agah − *Department of Electrical and Computer Engineering, Virginia Tech, Blacksburg, Virginia 24061, United States*

Inyoung Kim − *Department of Statistics, Virginia Tech, Blacksburg, Virginia 24061, United States*

Complete contact information is available at: https://pubs.acs.org/10.1021/acsanm.2c01644

Author Contributions

W.N. and W.Z. conceived the idea. W.N. fabricated SERS substrates, performed SERS measurements, and analyzed data. W.N., H.C., and I.K. performed machine learning analysis. X.R. and M.A. provided cells. W.N. and W.Z. wrote the manuscript.

Notes

The authors declare no competing financial interest.

ACKNOWLEDGMENTS

This work was supported by the Air Force Office of Scientific Research (AFOSR) Young Investigator Award FA9550-18-1-0328 and the National Cancer Institute (NCI) R21CA210216.

REFERENCES

(1) Wang, X.; Huang, S.-C.; Hu, S.; Yan, S.; Ren, B. Fundamental understanding and applications of plasmon-enhanced Raman spectroscopy. *Nature Reviews Physics* **2020**, *2* (5), 253−271.

(2) Zong, C.; Xu, M.; Xu, L. J.; Wei, T.; Ma, X.; Zheng, X. S.; Hu, R.; Ren, B. Surface-Enhanced Raman Spectroscopy for Bioanalysis: Reliability and Challenges. *Chem. Rev.* **2018**, *118* (10), 4946−4980.

(3) Xu, K.; Zhou, R.; Takei, K.; Hong, M. Toward Flexible Surface-Enhanced Raman Scattering (SERS) Sensors for Point-of-Care Diagnostics. *Adv. Sci. (Weinh)* **2019**, *6* (16), 1900925.

(4) Vikesland, P. J. Nanosensors for water quality monitoring. *Nat. Nanotechnol* **2018**, *13* (8), 651−660.

(5) Kuku, G.; Altunbek, M.; Culha, M. Surface-Enhanced Raman Scattering for Label-Free Living Single Cell Analysis. *Anal. Chem.* **2017**, *89* (21), 11160−11166.

(6) Nam, W.; Ren, X.; Tali, S. A. S.; Ghassemi, P.; Kim, I.; Agah, M.; Zhou, W. Refractive-Index-Insensitive Nanolaminated SERS Substrates for Label-Free Raman Profiling and Classification of Living Cancer Cells. *Nano Lett.* **2019**, *19* (10), 7273−7281.

(7) Song, J.; Nam, W.; Zhou, W. Scalable High-Performance Nanolaminated SERS Substrates Based on Multistack Vertically Oriented Plasmonic Nanogaps. *Adv. Mater. Technol.* **2019**, *4* (5), 1970028.

(8) Nam, W.; Song, J.; Safiabadi Tali, S. A.; Lezec, H. J.; Agrawal, A.; Zhou, W. Au/SiO2-Nanolaminated Plasmonic Nanoantennas as Refractive-Index-Insensitive and Transparent Surface-Enhanced Raman Spectroscopy Substrates. *ACS Appl. Nano Mater.* **2021**, *4*, 3175−3184.

(9) Huefner, A.; Kuan, W. L.; Muller, K. H.; Skepper, J. N.; Barker, R. A.; Mahajan, S. Characterization and Visualization of Vesicles in the Endo-Lysosomal Pathway with Surface-Enhanced Raman Spectroscopy and Chemometrics. *ACS Nano* **2016**, *10* (1), 307−316.

(10) Koike, K.; Bando, K.; Ando, J.; Yamakoshi, H.; Terayama, N.; Dodo, K.; Smith, N. I.; Sodeoka, M.; Fujita, K. Quantitative Drug Dynamics Visualized by Alkyne-Tagged Plasmonic-Enhanced Raman Microscopy. *ACS Nano* **2020**, *14* (11), 15032−15041.

(11) Kneipp, J. Interrogating Cells, Tissues, and Live Animals with New Generations of Surface-Enhanced Raman Scattering Probes and Labels. *ACS Nano* **2017**, *11* (2), 1136−1141.

(12) Khlebtsov, N.; Dykman, L. Biodistribution and toxicity of engineered gold nanoparticles: a review of in vitro and in vivo studies. *Chem. Soc. Rev.* **2011**, *40* (3), 1647−1671.

(13) Zito, G.; Rusciano, G.; Pesce, G.; Dochshanov, A.; Sasso, A. Surface-enhanced Raman imaging of cell membrane by a highly homogeneous and isotropic silver nanostructure. *Nanoscale* **2015**, *7* (18), 8593−8606.
(14) Xu, M.; Ma, X.; Wei, T.; Lu, Z. X.; Ren, B. In Situ Imaging of Live-Cell Extracellular pH during Cell Apoptosis with Surface-Enhanced Raman Spectroscopy. *Anal. Chem.* **2018**, *90* (23), 13922−13928.
(15) Han, Y.; Wu, S. R.; Tian, X. D.; Zhang, Y. Optimizing the SERS Performance of 3D Substrates through Tunable 3D Plasmonic Coupling toward Label-Free Liver Cancer Cell Classification. *ACS Appl. Mater. Interfaces* **2020**, *12* (26), 28965−28974.
(16) Zivanovic, V.; Milewska, A.; Leosson, K.; Kneipp, J. Molecular Structure and Interactions of Lipids in the Outer Membrane of Living Cells Based on Surface-Enhanced Raman Scattering and Liposome Models. *Anal. Chem.* **2021**, *93* (29), 10106−10113.
(17) Liang, O.; Wang, P.; Xia, M.; Augello, C.; Yang, F.; Niu, G.; Liu, H.; Xie, Y. H. Label-free distinction between p53+/+ and p53 −/− colon cancer cells using a graphene based SERS platform. *Biosens Bioelectron* **2018**, *118*, 108−114.
(18) La Rocca, R.; Messina, G. C.; Dipalo, M.; Shalabaeva, V.; De Angelis, F. Out-of-Plane Plasmonic Antennas for Raman Analysis in Living Cells. *Small* **2015**, *11* (36), 4632−4637.
(19) Lou, H. Y.; Zhao, W.; Li, X.; Duan, L.; Powers, A.; Akamatsu, M.; Santoro, F.; McGuire, A. F.; Cui, Y.; Drubin, D. G.; Cui, B. Membrane curvature underlies actin reorganization in response to nanoscale surface topography. *Proc. Natl. Acad. Sci. U. S. A.* **2019**, *116* (46), 23143−23151.
(20) Hanson, L.; Zhao, W.; Lou, H. Y.; Lin, Z. C.; Lee, S. W.; Chowdary, P.; Cui, Y.; Cui, B. Vertical nanopillars for in situ probing of nuclear mechanics in adherent cells. *Nat. Nanotechnol* **2015**, *10* (6), 554−562.
(21) Zhao, W.; Hanson, L.; Lou, H. Y.; Akamatsu, M.; Chowdary, P. D.; Santoro, F.; Marks, J. R.; Grassart, A.; Drubin, D. G.; Cui, Y.; Cui, B. Nanoscale manipulation of membrane curvature for probing endocytosis in live cells. *Nat. Nanotechnol* **2017**, *12* (8), 750−756.
(22) Abbott, J.; Ye, T.; Qin, L.; Jorgolli, M.; Gertner, R. S.; Ham, D.; Park, H. CMOS nanoelectrode array for all-electrical intracellular electrophysiological imaging. *Nat. Nanotechnol* **2017**, *12* (5), 460−466.
(23) Abbott, J.; Ye, T.; Krenek, K.; Gertner, R. S.; Ban, S.; Kim, Y.; Qin, L.; Wu, W.; Park, H.; Ham, D. A nanoelectrode array for obtaining intracellular recordings from thousands of connected neurons. *Nat. Biomed Eng.* **2020**, *4* (2), 232−241.
(24) Messina, G. C.; Dipalo, M.; La Rocca, R.; Zilio, P.; Caprettini, V.; Proietti Zaccaria, R.; Toma, A.; Tantussi, F.; Berdondini, L.; De Angelis, F. Spatially, Temporally, and Quantitatively Controlled Delivery of Broad Range of Molecules into Selected Cells through Plasmonic Nanotubes. *Adv. Mater.* **2015**, *27* (44), 7145−7149.
(25) Morais, C. L. M.; Lima, K. M. G.; Singh, M.; Martin, F. L. Tutorial: multivariate classification for vibrational spectroscopy in biological samples. *Nat. Protoc* **2020**, *15* (7), 2143−2162.
(26) Hinton, G.; Deng, L.; Yu, D.; Dahl, G.; Mohamed, A.-r.; Jaitly, N.; Senior, A.; Vanhoucke, V.; Nguyen, P.; Sainath, T.; Kingsbury, B. Deep Neural Networks for Acoustic Modeling in Speech Recognition: The Shared Views of Four Research Groups. *IEEE Signal Processing Magazine* **2012**, *29* (6), 82−97.
(27) Carrasquilla, J.; Melko, R. G. Machine learning phases of matter. *Nat. Phys.* **2017**, *13* (5), 431−434.
(28) Esteva, A.; Kuprel, B.; Novoa, R. A.; Ko, J.; Swetter, S. M.; Blau, H. M.; Thrun, S. Dermatologist-level classification of skin cancer with deep neural networks. *Nature* **2017**, *542* (7639), 115−118.
(29) Lussier, F.; Missirlis, D.; Spatz, J. P.; Masson, J. F. Machine-Learning-Driven Surface-Enhanced Raman Scattering Optophysiology Reveals Multiplexed Metabolite Gradients Near Cells. *ACS Nano* **2019**, *13* (2), 1403−1411.
(30) Thrift, W. J.; Ronaghi, S.; Samad, M.; Wei, H.; Nguyen, D. G.; Cabuslay, A. S.; Groome, C. E.; Santiago, P. J.; Baldi, P.; Hochbaum, A. I.; Ragan, R. Deep Learning Analysis of Vibrational Spectra of Bacterial Lysate for Rapid Antimicrobial Susceptibility Testing. *ACS Nano* **2020**, *14* (11), 15336−15348.
(31) Shin, H.; Oh, S.; Hong, S.; Kang, M.; Kang, D.; Ji, Y. G.; Choi, B. H.; Kang, K. W.; Jeong, H.; Park, Y.; Hong, S.; Kim, H. K.; Choi, Y. Early-Stage Lung Cancer Diagnosis by Deep Learning-Based Spectroscopic Analysis of Circulating Exosomes. *ACS Nano* **2020**, *14* (5), 5435−5444.
(32) Lussier, F.; Thibault, V.; Charron, B.; Wallace, G. Q.; Masson, J.-F. Deep learning and artificial intelligence methods for Raman and surface-enhanced Raman scattering. *TrAC Trends in Analytical Chemistry* **2020**, *124*, 115796.
(33) Boyd, M. R.; Paull, K. D. Some Practical Considerations and Applications of the National-Cancer-Institute in-Vitro Anticancer Drug Discovery Screen. *Drug Dev. Res.* **1995**, *34* (2), 91−109.
(34) Dobbelstein, M.; Moll, U. Targeting tumour-supportive cellular machineries in anticancer drug development. *Nat. Rev. Drug Discov* **2014**, *13* (3), 179−196.
(35) Johnson, P. B.; Christy, R. W. Optical Constants of the Noble Metals. *Phys. Rev. B* **1972**, *6*, 4370−4379.
(36) Mosmann, T. Rapid Colorimetric Assay for Cellular Growth and Survival - Application to Proliferation and Cyto-Toxicity Assays. *J. Immunol Methods* **1983**, *65* (1−2), 55−63.
(37) Le Ru, E. C.; Blackie, E.; Meyer, M.; Etchegoin, P. G. Surface enhanced Raman scattering enhancement factors: a comprehensive study. *J. Phys. Chem. C* **2007**, *111* (37), 13794−13803.
(38) McCreery, R. L. *Raman Spectroscopy for Chemical Analysis*; John Wiley & Sons, 2005. DOI: 10.1002/0471721646.
(39) Yang, J.; Xu, J.; Zhang, X.; Wu, C.; Lin, T.; Ying, Y. Deep learning for vibrational spectral analysis: Recent progress and a practical guide. *Anal. Chim. Acta* **2019**, *1081*, 6−17.
(40) Nam, W.; Zhao, Y.; Song, J.; Ali Safiabadi Tali, S.; Kang, S.; Zhu, W.; Lezec, H. J.; Agrawal, A.; Vikesland, P. J.; Zhou, W. Plasmonic Electronic Raman Scattering as Internal Standard for Spatial and Temporal Calibration in Quantitative Surface-Enhanced Raman Spectroscopy. *J. Phys. Chem. Lett.* **2020**, *11* (22), 9543−9551.
(41) Safiabadi Tali, S. A.; Song, J.; Nam, W.; Zhou, W. Two-Tier Nanolaminate Plasmonic Crystals for Broadband Multiresonant Light Concentration with Spatial Mode Overlap. *Advanced Optical Materials* **2021**, *9* (10), 2001908.
(42) Song, J.; Zhou, W. Multiresonant Composite Optical Nanoantennas by Out-of-plane Plasmonic Engineering. *Nano Lett.* **2018**, *18* (7), 4409−4416.
(43) Nam, W.; Kim, W.; Zhou, W.; You, E. A. A digital SERS sensing platform using 3D nanolaminate plasmonic crystals coupled with Au nanoparticles for accurate quantitative detection of dopamine. *Nanoscale* **2021**, *13* (41), 17340−17349.
(44) Deng, S.; Li, R.; Park, J. E.; Guan, J.; Choo, P.; Hu, J.; Smeets, P. J. M.; Odom, T. W. Ultranarrow plasmon resonances from annealed nanoparticle lattices. *Proc. Natl. Acad. Sci. U. S. A.* **2020**, *117* (38), 23380−23384.
(45) Liu, Y.; Zhang, Y.; Tardivel, M.; Lequeux, M.; Chen, X.; Liu, W.; Huang, J.; Tian, H.; Liu, Q.; Huang, G.; Gillibert, R.; de la Chapelle, M. L.; Fu, W. Evaluation of the Reliability of Six Commercial SERS Substrates. *Plasmonics* **2020**, *15* (3), 743−752.
(46) Volk-Draper, L. D.; Rajput, S.; Hall, K. L.; Wilber, A.; Rana, S. Novel model for basaloid triple-negative breast cancer: behavior in vivo and response to therapy. *Neoplasia* **2012**, *14* (10), 926−942.
(47) Weaver, B. A. How Taxol/paclitaxel kills cancer cells. *Mol. Biol. Cell* **2014**, *25* (18), 2677−2681.
(48) Nam, W.; Ren, X.; Kim, I.; Strobl, J.; Agah, M.; Zhou, W. Plasmonically Calibrated Label-Free Surface-Enhanced Raman Spectroscopy for Improved Multivariate Analysis of Living Cells in Cancer Subtyping and Drug Testing. *Anal. Chem.* **2021**, *93* (10), 4601−4610.
(49) Kneipp, K.; Haka, A. S.; Kneipp, H.; Badizadegan, K.; Yoshizawa, N.; Boone, C.; Shafer-Peltier, K. E.; Motz, J. T.; Dasari, R. R.; Feld, M. S. Surface-enhanced Raman Spectroscopy in single living cells using gold nanoparticles. *Appl. Spectrosc.* **2002**, *56* (2), 150−154.

(50) Krafft, C.; Neudert, L.; Simat, T.; Salzer, R. Near infrared Raman spectra of human brain lipids. *Spectrochim Acta A Mol. Biomol Spectrosc* **2005**, *61* (7), 1529−1535.
(51) Movasaghi, Z.; Rehman, S.; Rehman, I. U. Raman Spectroscopy of Biological Tissues. *Appl. Spectrosc. Rev.* **2007**, *42* (5), 493−541.
(52) Jordan, M. I.; Mitchell, T. M. Machine learning: Trends, perspectives, and prospects. *Science* **2015**, *349* (6245), 255−260.
(53) Acquarelli, J.; van Laarhoven, T.; Gerretzen, J.; Tran, T. N.; Buydens, L. M. C.; Marchiori, E. Convolutional neural networks for vibrational spectroscopic data analysis. *Anal. Chim. Acta* **2017**, *954*, 22−31.
(54) Ren, X.; Nam, W.; Ghassemi, P.; Strobl, J. S.; Kim, I.; Zhou, W.; Agah, M. Scalable nanolaminated SERS multiwell cell culture assay. *Microsyst. Nanoeng.* **2020**, *6* (1), 47.
(55) Huang, G.-B. Learning capability and storage capacity of two-hidden-layer feed-forward networks. *IEEE Trans Neural Netw* **2003**, *14* (2), 274−281.
(56) Hastie, T.; Tibshirani, R.; Friedman, J. *The elements of statistical learning*, 2nd ed.; Springer: New York, 2009; p 33. DOI: 10.1007/978-0-387-84858-7_2.
(57) Noble, W. S. What is a support vector machine? *Nat. Biotechnol.* **2006**, *24* (12), 1565−1567.
(58) Ben-David, U.; Siranosian, B.; Ha, G.; Tang, H.; Oren, Y.; Hinohara, K.; Strathdee, C. A.; Dempster, J.; Lyons, N. J.; Burns, R.; Nag, A.; Kugener, G.; Cimini, B.; Tsvetkov, P.; Maruvka, Y. E.; O'Rourke, R.; Garrity, A.; Tubelli, A. A.; Bandopadhayay, P.; Tsherniak, A.; Vazquez, F.; Wong, B.; Birger, C.; Ghandi, M.; Thorner, A. R.; Bittker, J. A.; Meyerson, M.; Getz, G.; Beroukhim, R.; Golub, T. R. Genetic and transcriptional evolution alters cancer cell line drug response. *Nature* **2018**, *560* (7718), 325−330.

https://doi.org/10.1021/acsanm.2c01644
ACS Appl. Nano Mater. 2022, 5, 10358−10368